Pergamon

Int. J. Multiphase Flow Vol. 24, No. 4, pp. 587–603, 1998

Printed in Great Britain

PII: S0301-9322(97)00070-0

0301-9322/98 $19.00 + 0.00

PREDICTION OF THE EFFECTS OF LIQUID VISCOSITY ON INTERFACIAL SHEAR STRESS AND FRICTIONAL PRESSURE DROP IN VERTICAL UPWARD GAS–LIQUID ANNULAR FLOW

T. FUKANO[1] and T. FURUKAWA[2]

[1]Kyushu University, Hakozaki, Fukuaka 812, Japan
[2]Sasebo College of Technology, Sasebo, Nagasaki 857-11, Japan

(Received 6 March 1997; in revised form 17 September 1997)

Abstract—The purpose of the present study is to investigate the effects of liquid viscosity on the mean liquid film thicknesses, wave heights, and gas–liquid interfacial shear stresses in the vertical-upward co-current annular flow in a 26.0 mm inner diameter tube. Water and glycerol solutions were used as working fluids to change the kinematic viscosity of liquid from 0.85×10^{-6} to 8.6×10^{-6} m^2/s. The mean liquid film thicknesses and wave heights were determined using the signals of time-varying cross-sectionally averaged holdup which were detected by a constant current method at a distance of about 3.5 m from an air–liquid mixer. The pressure gradients were also measured by a U-tube manometer. As a result we proposed correlations for the mean liquid film thicknesses and the interfacial friction factors. In addition a method to estimate the pressure drops is proposed and verified that the calculated values are in good agreement with the measured values. © 1998 Elsevier Science Ltd. All rights reserved

Key Words: multiphase flow, annular flow, vertical upward flow, liquid viscosity, mean liquid film thickness, pressure drop, wave height, interfacial friction factor

1. INTRODUCTION

Gas–liquid annular two-phase flow, in which liquid film with waves of various sizes flows on the wall, and gas phase flows in the center of the tube with an extremely larger velocity than the liquid film, is frequently encountered in many industries which use steam generators in power plants, various boilers, pipe-lines carrying wet steam, chemical contacting equipment and air conditioners. Various types of fluid are used in these appliances. However, among the many reports (for example, Abolfadl and Wallis, 1986; Jensen 1987; Skouloudis and Würtz 1993) few treat the effect of physical properties of fluid on the liquid film flow.

The present authors have already reported on the detailed structure of the gas–liquid interface, which is shown as the time-spatial characteristic maps of gas–liquid interfaces (Furukawa, 1995; Furukawa and Fukano 1996). From these maps it has been clarified that the gas–liquid interfacial structure is significantly influenced by the liquid viscosity. The interfacial shear stress, which is closely related to the gas–liquid interfacial structures, is strongly related, for example, to the heat transfer characteristics of the liquid film flow.

The objectives of this paper are to investigate the effects of liquid viscosity on the interfacial shear stress, the mean film thickness and the wave height, and to propose their correlations and method to predict the pressure drops by using the proposed correlations.

The experiments were performed using water and aqueous glycerol solutions as working liquids with a 10-time difference in liquid viscosity for isothermal co-current air–liquid vertical flow in a 26.0 mm and 19.2 mm inner diameter tubes.

2. EXPERIMENTAL APPARATUS

Figure 1 shows the schematic view of a test tube 26.0 mm in diameter (D) and about 4.6 m in length. It was made of transparent acrylic resin, and vertically set up. Air and four different

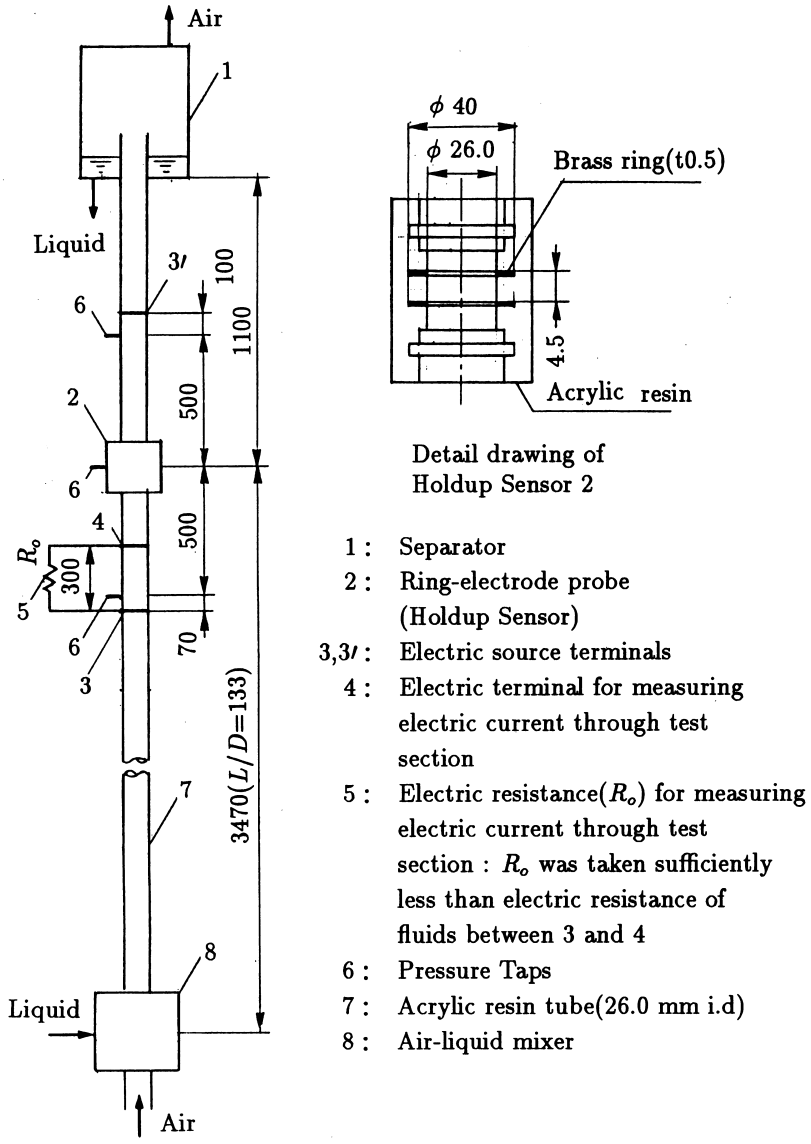

Figure 1. Schematic diagram of the experimetal setup.

liquids, i.e., water and aqueous glycerol solutions with different liquid viscosity, were employed as the test fluids. Their properties are shown in table 1.

An air–liquid mixer, 8, consisted of a double tube (80 mm in length), the inner diameter of which was the same as that of the test tube. The air was blown into the inner tube through 60 holes with 2 mm diameter.

The air–liquid mixture flowed vertically upwards via the measuring section 2, the distance of which was about 3.5 m (L/D = 133) from the mixer (L), into an air–liquid separator 1 located at 1.1 m downstream of the measuring section. The air was discharged into atomosphere, and the liquid was returned back to a liquid storage tank.

The time-varying liquid film thickness was measured by using a holdup sensor installed in the measuring section. As shown in detail in the right-upper part of figure 1, the holdup sensor was composed of a pair of brass rings with the thickness of 0.5 mm, and these rings were embedded flush with the inner surface of tube with nonconductive acrilic resin of 4.5 mm thickness between them. The measured value of the film thickness was then averaged over 4.5 mm axial length as well as circumferentially. The constant current method developed by Fukano (1997) was used to measure the liquid holdup. A summary of this method was also described in previous papers

Table 1. Physical properties of liquids used in the experiments

Liquid		v_L m^2/s	ρ_L kg/m^3	σ_L N/m
Water	(W09)	0.85×10^{-6}	998	7.2×10^{-2}
45 wt% Glycerol soln	(G3)	3.4	1113	6.5
53 wt% Glycerol soln	(G5)	5.6	1149	6.2
60 wt% Glycerol soln	(G9)	8.6	1159	6.6

v_L: kinematic viscosity, ρ_L: density, σ_L: surface tension.

(Furukawa 1995; Fukano 1997). The time-varying, cross-sectionally averaged liquid holdup signals from the constant current holdup sensors were calculated by a computer to obtain the mean liquid film thickness and the wave height.

Three pressure taps 6 were installed at three axially different locations with the spacing of 0.5 m, the center of which was located at the holdup measuring section. These pressure taps were used to measure the system pressures and the pressure drops in 1 m axial lengths.

The experimental conditions were as follows: superficial gas velocity j_G: $10 \sim 50$ m/s, superficial liquid velocity j_L: $0.04 \sim 0.3$ m/s, system pressure: $0.103 \sim 0.117$ MPa, and air and liquid temperature: $27 \sim 29^\circ$C. The liquid viscosity was measured before and after the experiments and it was almost the same. The change between the liquid flow rate due to evaporation and the gas flow was estimated to be less than 1% in the most extreme case and it did not cause appreciable change of the liquid viscosity.

3. EXPERIMENTAL RESULTS AND DISCUSSION

3.1. *Visual observations of the flow by still photographs and the shapes of waves taken by the liquid holdup sensors*

Figure 2 shows the still photographs (figure 2(1)) and the time-varying cross-sectionally averaged liquid holdup signals (figure 2(2)) (referred to as the η-signal in this paper) for four kinds of liquid viscosity v_L under the same gas and liquid flow conditions, $j_G = 40$ m/S, $j_L = 0.04$ m/s. Figure 2(a) is for the air–water system, and (b), (c) and (d) for the air–aqueous glycerol solution systems in which kinematic viscosity of liquid v_L are 0.85×10^{-6}, 3.4×10^{-6}, 5.6×10^{-6} and 8.6×10^{-6} m^2/s, respectively. These are referred to as W09, G3, G5 and G9, respectively. The sign SW in figure 2 represents the small wave and LW the large wave. Fukano *et al.* (1983) have proposed a flow model for a liquid film flow in a horizontal air–water annular flow. According to this flow model, the liquid film flow consists of disturbance waves and a continuous liquid film. The liquid film is named as a base film, and the ripples formed on the base film are named as base waves. LW used in this paper corresponds to the disturbance wave in air–water system. As discussed in previous papers (Furukawa, 1995), the reason the term LW is used is that LW, in the case of liquid with higher viscosity, shows different velocity characteristics, as clearly shown in the spatial distribution of waves in comparison with the disturbance wave in air–water system. In addition, SW is used as synonymous with the base wave.

LW seen in figure 2(1)(a) and (b) corresponds to the triangular wave form with high peck values in figure 2(2)(a) and (b). As shown in figure 2(2)(a) – (d), the passing frequency of LW decreases remarkably with increasing v_L, and LW cannot be observed in G9, where the flow pattern is ripple flow (Furukawa, 1995).

In the case of W09, as seen in figure 2(1) and (2), the wave height of the small waves (SW) formed on the base film is so small and the interface of base film in W09 looks smooth. On the other hand the existence of SW becomes more and more clear as v_L increases, and the fluctuation of film thicknesses with time also becomes stronger as clearly seen in figure 2(2)(d).

As seen from these examples, the appearance of the wavy surface clearly changes with v_L even under the same flow conditions of gas and liquid. This fact suggests that the interfacial friction factor, which will be closely related to the wave characteristics, is considerably affected by v_L.

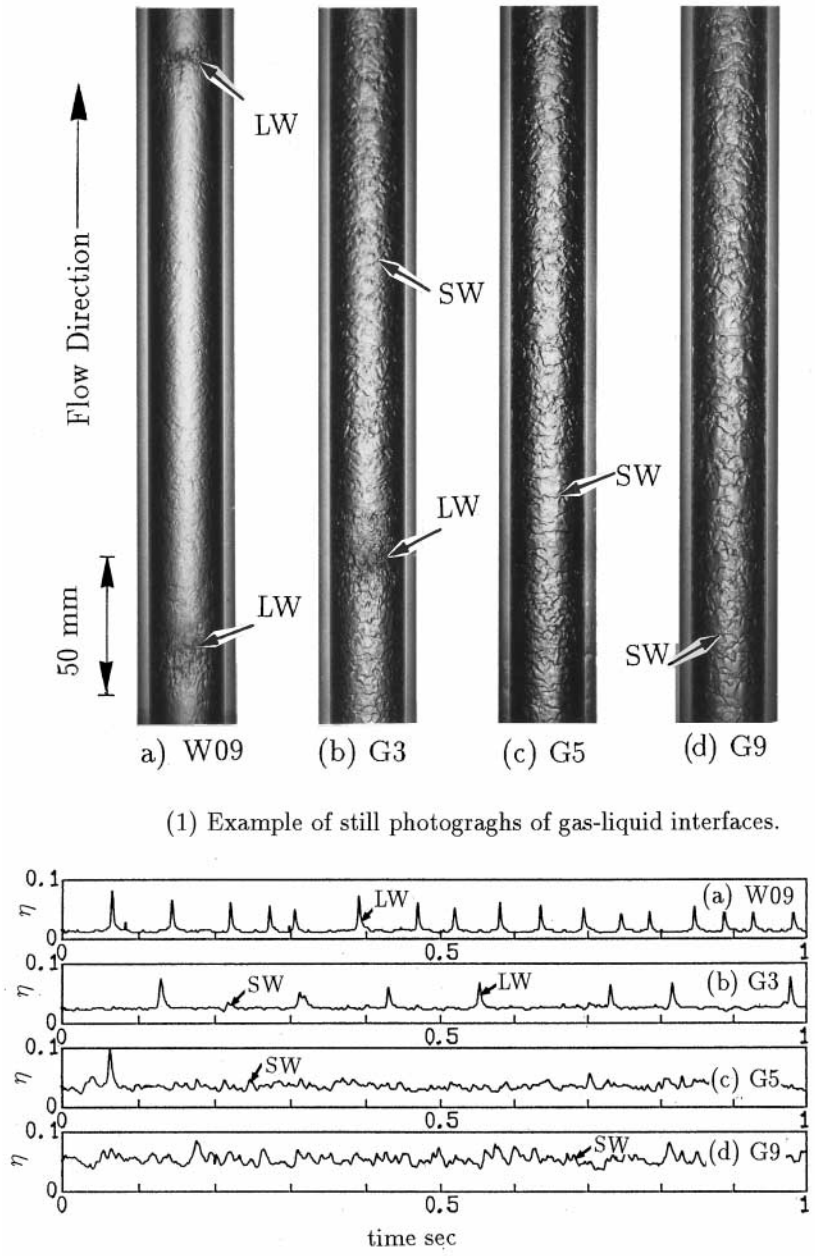

Figure 2. Effect of liquid viscosity on gas–liquid interfacial structure ($j_G = 40$ m/s, $j_L = 0.04$ m/s). (1) Example of still photograghs of gas–liquid interfaces. (2) Example of time-varying cross-sectionally averaged liquid holdup signals η.

3.2. *Range of experiment and flow patterns*

Weisman and Kang (1981) investigated the boundaries of the flow patterns mainly based on the superficial velocities of both phases, and in some part examined the effects of liquid viscosity on flow pattern transition. They, however, classified the flow patterns into annular and intermittent, if we limited the flow rate conditions within our experimental range. In this study the transition zone between those two resions corresponds to the **FA–F** boundary, where the effects of the viscosity is not clear, as will be discussed later.

Baker's flow pattern map (Baker 1954) is another example where the fluid property is taken into consideration although, in this case, for horizontal flow. Figure 3 shows the range of our experiment and the boundaries of the flow patterns plotted on the Baker's map. The ordinate of this map is the ratio of mass flow rate of gas (G_G) to λ, and the abscissa the product of three

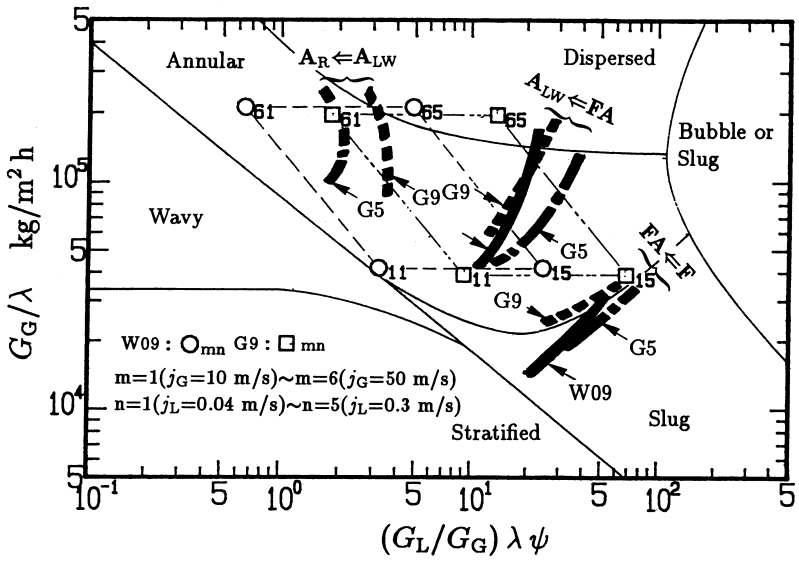

Figure 3. Experimental ranges and flow patterns.

values, the ratio of mass flow rate of liquid (G_L) to gas G_L/G_G, λ, and ψ. λ and ψ are defined as follows:

$$\lambda = \{(\rho_G/\rho_A)(\rho_L/\rho_W)\}^{\frac{1}{2}} \quad [1]$$

$$\psi = (\sigma_W/\sigma_L)\{(\nu_L/\nu_W)(\rho_W/\rho_L)\}^{\frac{1}{3}} \quad [2]$$

where ρ, σ and ν are the density, the surface tension, and the kinematic viscosity, respectively. The subscripts L, W, G, and A stand for liquid, water at 20°C, gas, and air at 0.101 MPa and 20°C, respectively. The flow pattern map expressed by thin solid lines has been proposed by Baker (1954). One of the reasons for comparing the flow pattern boundaries in the vertical pipe with the Baker map is that annular flow is considered to be relatively independent of the direction of gravitational accerelation.

The marks ○ and □ in figure 3, respectively show the experimental range for W09, where v_L is the smallest, and G9, where v_1 is the largest. Although the experimental range of G9 moves right from that of W09, even under the same gas and liquid flow conditions due to the difference in v_L, the flow patterns observed in the present experiments were always annular but annular and dispersed flow regions are found in the horizontal flow method by Baker.

Thick solid lines, one-dot chain lines, and broken lines represent the boundaries of the flow patterns obtained in the present experiments for W09, G5 and G9, respectively. Both boundaries between the annular flow accompanied by LW($\mathbf{A}_{LW}$) and the ripple flow ($\mathbf{A}_R$), and between the froth-annular flow (**FA**) and $\mathbf{A}_{LW}$ were classified by direct visual observation of the flow configuration as well as indirect visual observations using still photographs, video, or wave forms of signals of the cross-sectional mean liquid holdup (η). The boundary between **FA** and $\mathbf{A}_{LW}$ is almost the same as in the case of 19.2 mm i.d. reported by Furukawa and Fukano (1996).

As described in the paper by Furukawa and Fukano (1996), the classification of the flow pattern into **FA** and $\mathbf{A}_{LW}$ was based on the behavior of LW which flows intermittently, as if sliding on the base film. The flow is classified into $\mathbf{A}_{LW}$ if the velocity, size, and axial spacing of each large wave (LW) appeared on the annular liquid film as comparatively uniform. On the other hand, the flow is classified into **FA** if the velocity and so on are not uniform because the flow is considered not to be fully-developed although the flow should be judged as annular according to the conventional classification method because of the disappearance of liquid slugs which cover the whole cross-section of the tube.

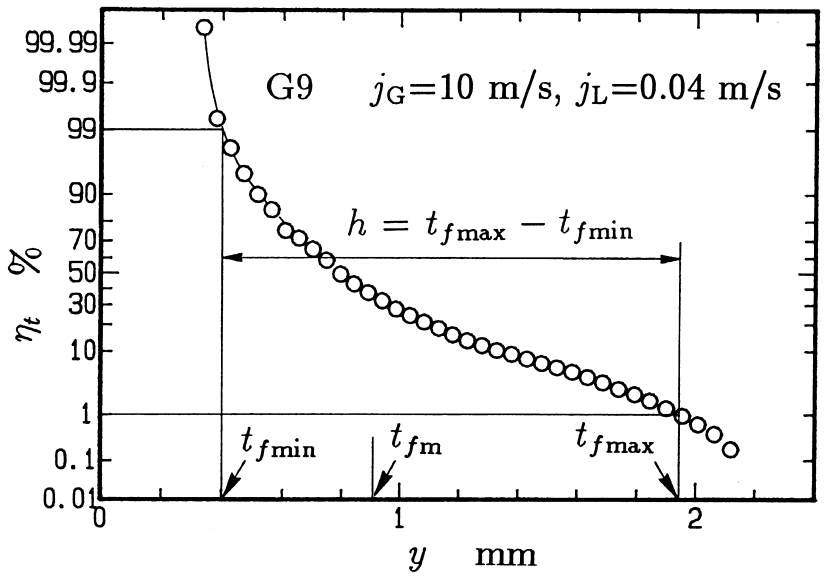

Figure 4. Definitions of the ratio of existence time of liquid phase η_t, the maximum and the minimum liquid film thickness $t_{f\max}$ and $t_{f\min}$ and the wave height h.

The boundary between froth flow (**F**) and **FA**, which corresponds to the disappearance of liquid slugs, was determined based on the result of a previous paper (Furukawa and Fukano, 1996).

3.3. *Liquid film thickness and its correlation*

3.3.1. *Definition of liquid film thickness and wave height*. The mean liquid film thickness (t_{fm}) was determined by substituting the mean value of the time fluctuating holdup, $\bar{\eta}$, sampled by A–D converter at 3 kHz frequency over 20 sec, as the following equation.

$$t_{fm} = (D/2)(1 - \sqrt{1 - \bar{\eta}}) \quad [3]$$

Figure 4 shows a ratio of existence time of liquid phase (η_t) to total sampling time of η-signals plotted on a normal probability paper in the case of, for example, G9, $j_G = 10$ m/s, and $j_L = 0.04$ m/s. Abcissa y is the distance from the wall surface. In figure 4, the values of y at $\eta_t = 99\%$ and 1% are defined as the minimum and the maximum film thickness, respectively, and the difference of these film thicknesses is defined as the wave height.

Figure 5 shows the mean liquid film thickness if t_{fm} plotted against j_G while keeping j_L constant. Parameter is v_L. Figure 5(a), (b) and (c) correspond to the cases of $j_L = 0.04$, 0.06, and 0.1 m/s, respectively. Symbols of ○, ▽, △ and □ represent W09, G3, G5 and G9, respectively (symbols used in all the figures in this paper have the same significance). The solid lines (used for expressing the case of W09), broken lines (G3), one-dot chain lines (G5), and dotted lines (G9) in the figures represent [9] discussed later.

As shown in figure 5, t_{fm} asymptotically decreases with increasing j_G regardless of the magnitude of v_L and j_L. The t_{fm} is strongly affected by v_L, i.e., it increases with v_L under the same conditions as j_G and j_L.

Figure 6 shows the wave height h which is measured under the same flow conditions as whose shown in figure 5. It is seen that the wave height h decreases monotonically with increasing j_G, and the effect of v_L on the h is not clear except in the large j_L case, where there is an increasing tendency of h with v_L (figure 6(c)). The flow patterns at the experimental points shown by solid symbols ▲ and ■ in the case of G5 and G9 were identified as the ripple flow (see figure 2) since the large wave LW was scarcely observed. This means that although the wave heights in these cases of G9 for $j_G = 40$ and 50 m/s correspond to those of the small wave SW, these values are approximately equal to the wave height of the large wave LW for W09. The difference of wave

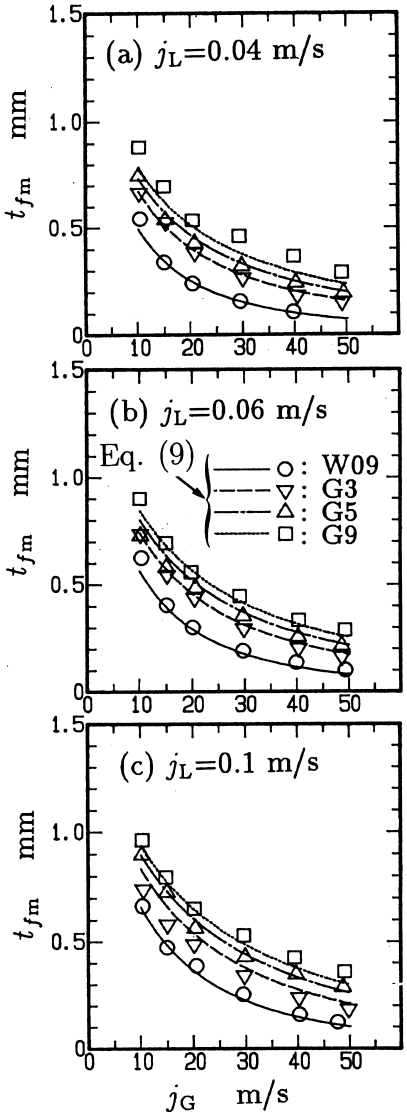

Figure 5. Relation between the mean liquid film thicknesses t_{fm} and the superficial gas velocities.

characteristics between G9 and W09 is visually observed, for example, in figure 2. The half solid symboles in figure 6(c) will be referred to in Section 3.

In figure 7 the contour lines of the mean liquid film thickness are shown by thin solid lines and the wave height by thin one-dot chain lines on the j_G–j_L chart in the case of, for example, G5. The thick solid lines are the boundaries of each flow pattern. The mean liquid film thickness t_{fm} increases with increasing j_L, and decreases with increasing j_G. Meanwhile, although the wave height h becomes independent of j_L, and depends only on j_G in the vicinity of the boundary between **FA** and $\mathbf{A}_{LW}$, the effect of j_L on h gradually appears as j_G increases, and the contour line of h becomes parallel with the contour line of t_{fm} in the region of $j_G \cong 30$–50 m/s. That is, the wave height is proportional to the mean liquid film thickness, and the contour line of $h = 0.3$ mm approximately agrees with the boundary between $\mathbf{A}_{LW}$ and $\mathbf{A}_R$ as clearly seen in figure 7. in the case of small j_L and high j_G. The same tendency described above is seen in the cases of other values of v_L.

In order to clarify the reason for differences in the slopes of the contour lines of the mean liquid film thickness and the wave height, detailed investigation of the wavy characters, such as passing frequency of LW, velocity of LW and so on, is required.

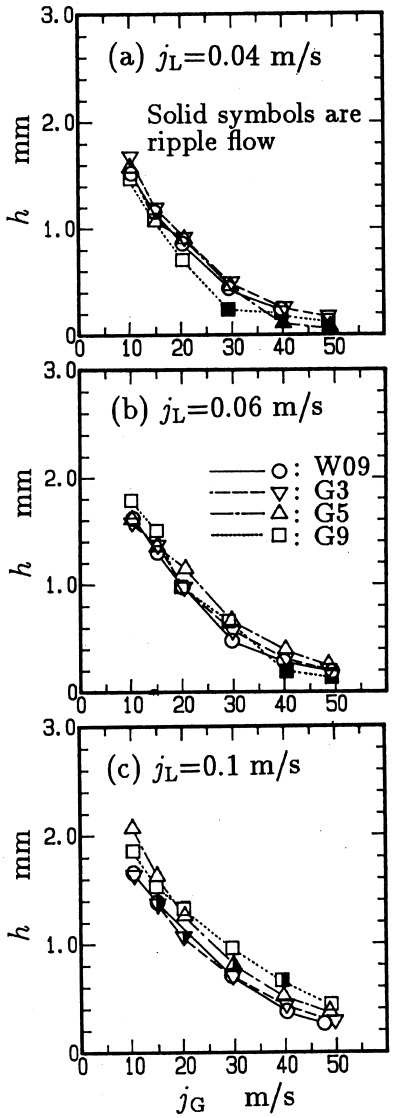

Figure 6. Relation between the wave height h and the superficial gas velocities.

3.3.2. *Correlation of the mean liquid film thickness*. The holdup or the mean liquid film thickness t_{fm}, is the most fundamental parameter of the liquid film flow. Ambrosini *et al.* (1991) investigated the correlation for film thickness by using data of their own, Willetts (1987), Asali *et al.* (1985) Leman (1983), Leman (1985), Whalley *et al.* (1973), Whalley and Hewitt (1978) and Gill *et al.* (1964), Gill *et al.* (1969), and recommend the following relation proposed by Asali *et al.* (1985).

$$m_L^+ = 0.34 Re_{LF}^{0.6} \quad [4]$$

for $Re_{LF}\langle 1000$, and the next relation proposed by Kosky (1971)

$$m_L^+ = 0.0512 Re_{LF}^{0.875} \quad [5]$$

for $Re_{LF}\rangle 1000$. The dimensionless thickness, m_L^+, and the liquid film Reynolds number, Re_{LF}, are defined as

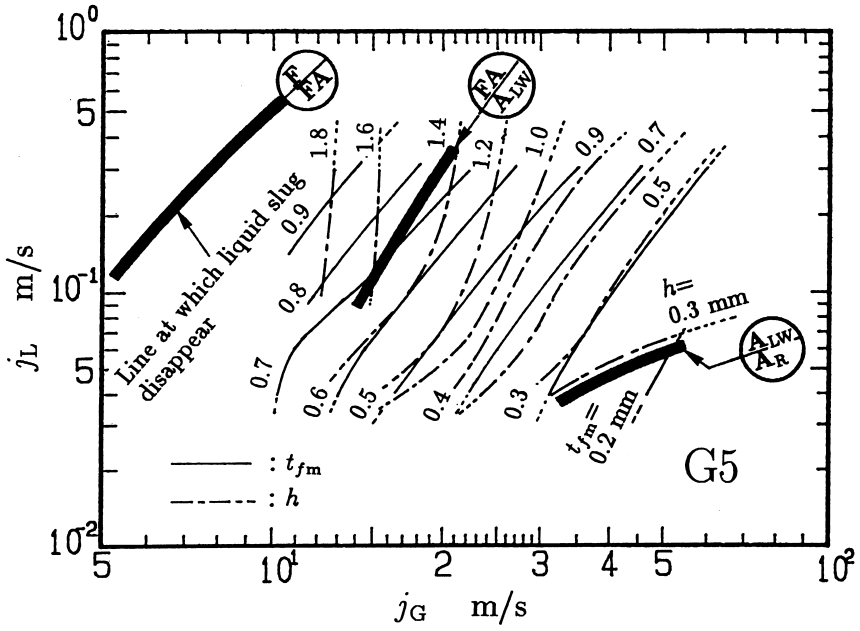

Figure 7. Contour maps of the mean liquid film thickness and the wave height in the case of G5.

$$m_L^+ = \frac{t_{fm} U_L^*}{\nu_L} \qquad [6]$$

and

$$Re_{LF} = \frac{4\Gamma_M}{\mu_L} \qquad [7]$$

where Γ_M is the mass flow rate of liquid film per unit width of wall surface, and μ_L the dynamic

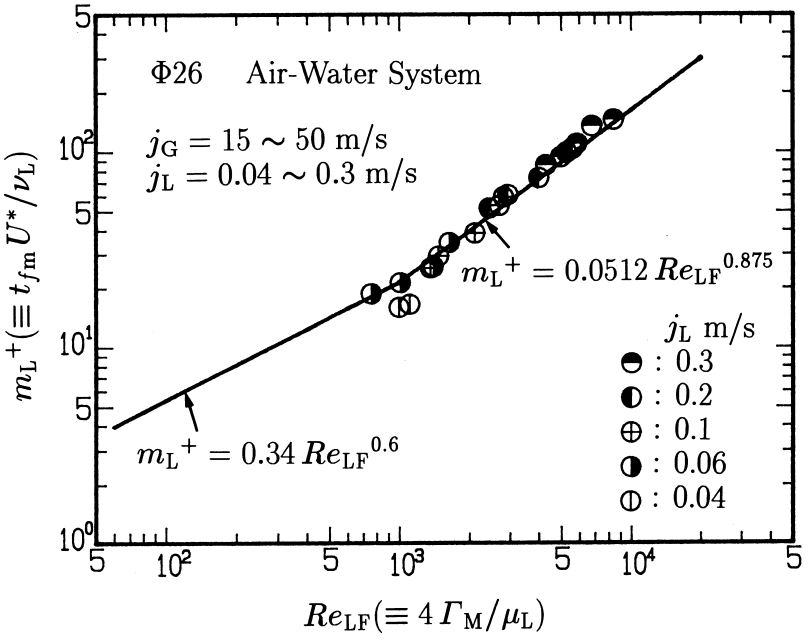

Figure 8. Mean liquid film thickness prediction. (Nishikawa *et al.*'s entrainment data (tube dia. = 25.1 mm) were used.)

viscosity. It is noticed that the entrainment data, are necessary to calculated Γ_M. The liquid friction velocity, U_L*, which is used for the calculation of the dimensionless film thickness, m_L^+, is defined by

$$U_L^* = \sqrt{\frac{\tau_c}{\rho_L}} \quad [8]$$

where τ_c is a characteristic shear stress, and approximately equal to the interfacial shear stress, τ_i, at high gas velocity.

Figure 8 shows the comparison of the present author's data, with those correlations, [4) and (5], for air–water flow, where the Nishikawa *et al.*'s data (1967) was used for calculation of the entrainment flow rate. Similar comparison was made in figure 9, where Asah's entrainment data (1984) was used. Both figures show that the correlations for m_L^+ are quite useful to accurately estimate film thickness for air–water flow obtained in this study. Those figures also show that the film thickness data obtained in this experiment are within a scatter of data given by other authors, as described above, even when the values of Re_{LF} were calculated by using the different authors' data. This fact verifies that the present film thickness data is useful.

On the other hand correlations for the entrainment flow rate must be used for any kind of liquid with different viscosity to estimate film thickness by using [4) and (5]. Such correlations, however, are not, as yet, available. We endeavoured to introduce the correlation for film thickness from a different point of view, and obtained the following correlation, [9], to estimate t_{fm}, which was obtained by trial and error.

$$t_{fm}/D = 0.0594\exp(-0.34 Fr_{GO}^{0.25} Re_{LO}^{0.19} x^{0.6}) \quad [9]$$

Where Fr_{GO} is the Froude number defined by superficial velocity of gas phase ($\equiv j_G/\sqrt{gD}$, g is acceleration of gravity), Re_{LO} the Reynolds number defined by superficial velocity of liquid phase ($\equiv j_L\ D/\nu_L$), x the quality ($\equiv j_G\ \rho_G/(j_G\ \rho_G + j_L\ \rho_L)$). The curves shown in figure 5(a)–(c) are calculated by [9] for the corresponding liquid viscosity. The measured values agreed well with the experimental data. Comparisons of the measured values with the calculated values for all the flow conditions tested are shown in figure 10. Similar comparisons of the present experimental data with the correlation, [10] proposed by Hori *et al.* (1978), are also shown in the

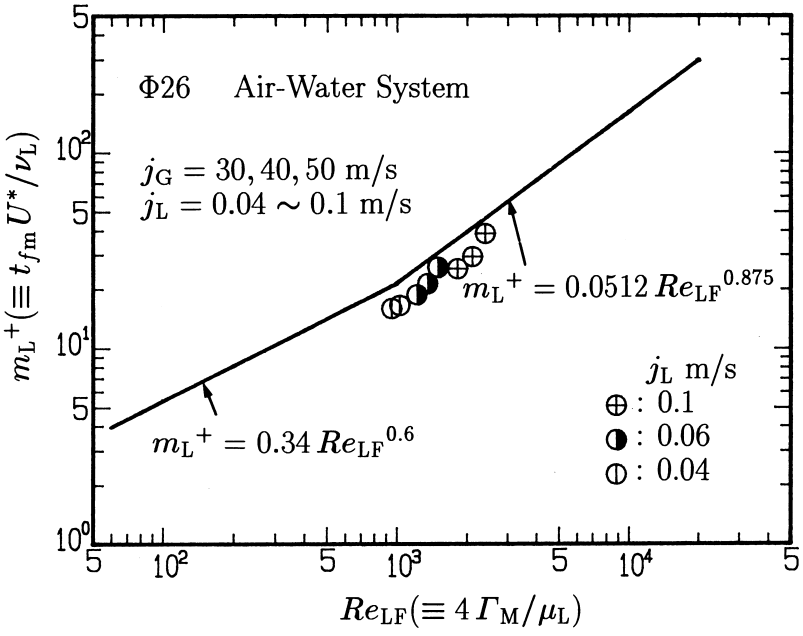

Figure 9. Mean liquid film thickness prediction. (Asali's entrainment data (tube dia. = 22.9 mm) were used.)

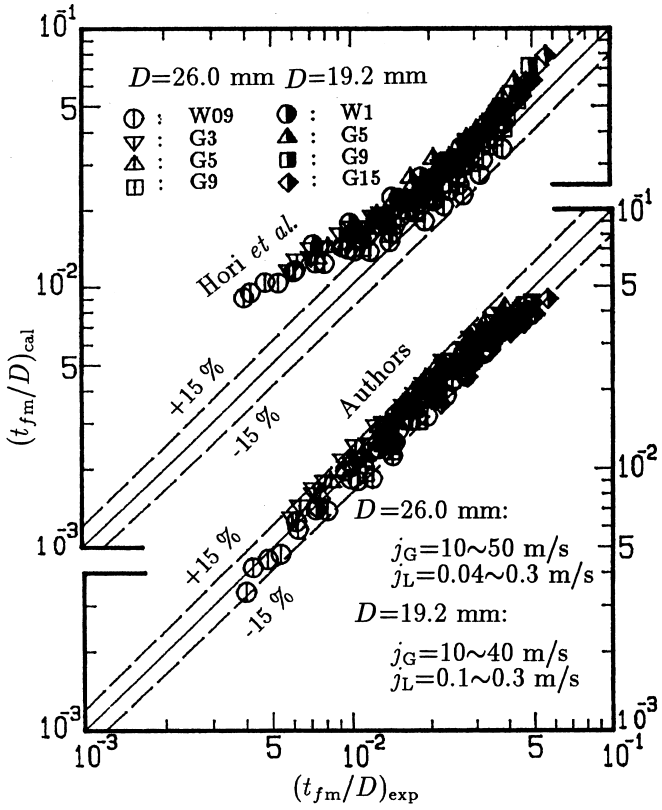

Figure 10. Comparison of the relative mean liquid film thicknesses t_{fm}/D between measured and calculated.

upper part of figure 10.

$$t_{fm}/D = 0.905 Re_{GO}^{-1.45} Re_{LO}^{0.90} Fr_{GO}^{0.93} Fr_{LO}^{-0.68} (\mu_L/\mu_W)^{1.06} \quad [10]$$

Where, $Fr_{LO} \equiv j_L/\sqrt{g\,D}$, $Re_{GO} \equiv j_G\,D/\nu_G$. μ_L and μ_w are the viscosity of liquid used and water at 20°C, respectively.

As seen in figure 10, the correlation by Hori *et al.* (1978) gives larger values especially where t_{fm}/D becomes small. On the other hand the authors' correlation estimates t_{fm} with the accuracy of ±15% in the whole range of the present experimental flow conditions.

3.4. *Interfacial friction factor* λ_i

3.4.1. *Definition of* λ_i *and its general trend.* Based on the flow of gas occupying the center part of the tube, the relationship between the pressure drop $(-dp/dz)$ and the interfacial shear stress τ_i for the fully-developed gas flow is obtained by a force balance as follows:

$$-\frac{dp}{dz} = 4\frac{\tau_i}{D_i} + \rho_G g \quad [11]$$

where D_i is the diameter of gas–liquid interface ($D_i \equiv D - 2t_{fm}$), and ρ_G and g are the density of gas and the gravitational accerelation, respectively.

Meanwhile the interfacial friction factor λ_i, which is equivalent to τ_i, is defined by the following equation,

$$\lambda_i = \frac{8\tau_i}{\rho_G(\bar{u}_G - u_i)^2} \quad [12]$$

where $\bar{u}_G$ is the mean absolute velocity of the gas phase, i.e., $\bar{u}_G = j_G/\hat{\alpha}$ and $\hat{\alpha}$ is the cross-sectionally averaged void fraction, and is obtained by $\hat{\alpha} = (D_i/D)^2$ in the case of negligible entrainments.

It is assumed that the interfacial velocity u_i is equal to the interfacial wave velocity. According to the measured values, the wave velocities, in the case of the annular flow, are much smaller than the averaged gas velocity $\bar{u}_G$. Furthermore, the 2nd term on the right hand side of [11] is at most 1% of the 1st term, and negligibly small. Then if we respectively neglect u_i in [12] and the 2nd term in [11], λ_i is calculated by the following equation by substituting the measured values of D_i, $-dp/dz$, and $\bar{u}_G$.

$$\lambda_i = \frac{2D_i(-dp/dz)}{\rho_G \bar{u}_G^2} \qquad [13]$$

Figure 11 shows λ_i calculated from [13] for each v_L as a function of the measured relative mean liquid film thicknesses nondimensionalized by the tube diameter D, t_{fm}/D in the case of $j_L = 0.1$ m/s, for example. The four thin lines in figure 11 represent the correlation [19] of λ_i for different v_L as described later.

In this figure it shown is that λ_i increases rapidly regardless of v_L with increasing film thicknesses, because the interfacial roughness increases due to the increases of t_{fm} and h with decreasing j_G, as already shown in figures 5 and 6. Moreover, it is found that λ_i becomes small with increasing v_L if they are compared under the same value of the liquid film thicknesses. One of the reasons for this is that the wave height decreases with increasing v_L. For example, if the data expressed by the half solid symbols in figures 11 and 6(c), which were taken in the same gas and liquid flow-rate conditions, are compared it is clear that the wave heights become smaller as v_L increases, as seen in figure 6(c) although the liquid film thicknesses take almost the same values v_1 as seen in figure 11.

3.4.2. *Correlation of λ_i.* The thick broken line and the one-dot chain line in figure 11 represent the following correlations, [14] and [15], proposed by Wallis (1969) and Moeck (1970), respectively. The data used for the correlation (15) were obtained for the disturbance wave region of the air–water annular flow.

$$\lambda_i = 0.02\{1 + 300(t_{fm}/D)\} \text{ (Wallis)} \qquad [14]$$

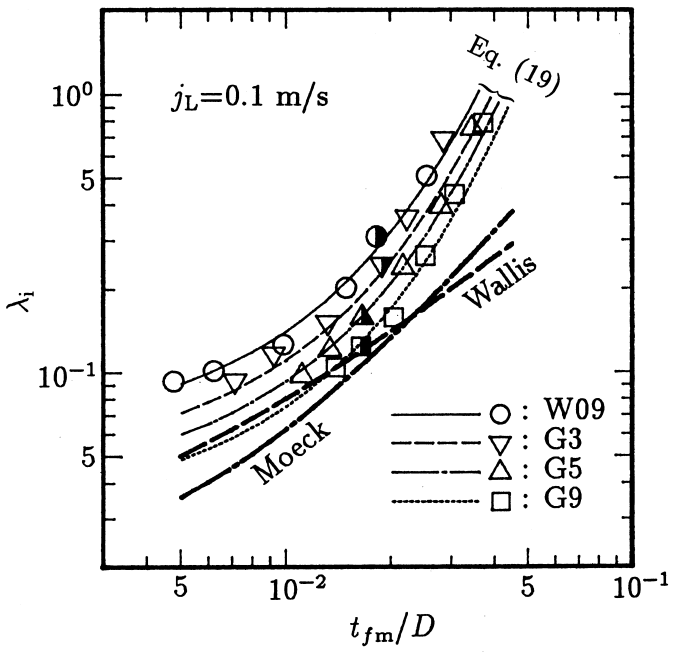

Figure 11. Relation between the relative mean liquid film thicknesses t_{fm}/D and the interfacial friction factor λ_i.

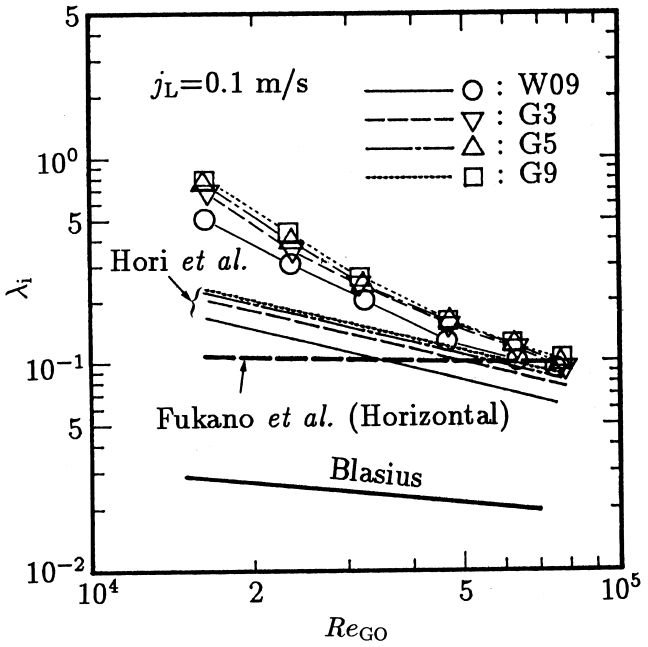

Figure 12. Interfacial friction factor λ_i against superficial gas Reynolds number Re_{GO}.

$$\lambda_i = 0.02\{1 + 1458(t_{fm}/D)^{1.42}\} \text{ (Moeck)} \quad [15]$$

It is clearly shown in figure 11 that both the above correlations estimate smaller values than the present experimental data. We used the constant current method to measure the holdup, where it is possible for the measured film thickness to be a little smaller than the actual one if the bubbles or gas phase are included in the liquid film flow. Even if this is true, our data is within the scatter of other researchers' data as discussed in the Section 3.3.2 *Correlation of the mean liquid film thickness*, although the difference in λ_i between our findings and those of Wallis [14] and Moeck [15] is not clear.

Figure 12 shows the experimental data of λ_i plotted as a function of the superficial gas Reynolds number Re_{GO}. It is clearly shown in this figure that the experimental values of λ_i, designated by ○ (W09), ▽ (G3), △ (G5), and □ (G9), monotonically decrease with increasing Re_{GO} irrespective of v_L, while the λ_i increases slightly as v_L increases in the whole range of Re_{GO}. The reason of this is that the wave height increases with v_L as already shown in figure 6. The thick solid line in the lower part of this figure expresses the Blasius's equation given by the next equation for a single phase flow in a smooth inner tube surface.

$$\lambda_S = 0.316 Re_G^{-0.25} (= 0.316 Re_{GO}^{-0.25}) \quad [16]$$

Where Re_G is the Reynolds number defined by $\bar{u}_G$ ($\equiv \bar{u}_G\, D/v_G$). The difference of values calculated by the above [16] for Re_G and Re_{GO} is within 5% and negligible. It is clearly shown in figure 12 that the interfacial friction factor λ_i for gas–liquid two-phase annular flow is significantly larger than the values given by the Blasius's equation. A group of lines designated as Hori *et al.* (1978) is given by the following equation:

$$\lambda_i = 1.13 Re_{GO}^{-0.89} Re_{LO}^{0.68} Fr_{GO}^{0.25} Fr_{LO}^{-0.45} (\mu_L/\mu_W)^{0.77} \quad [17]$$

The estimated values for this equation are considerably smaller than the present experimental values in the lower Re_{GO} region and approach the present data in the high Re_{GO} region.

On the other hand, the thick broken line represents the following correlation proposed by Fukano *et al.* (1985) for thin water film flow in a horizontal rectangular duct.

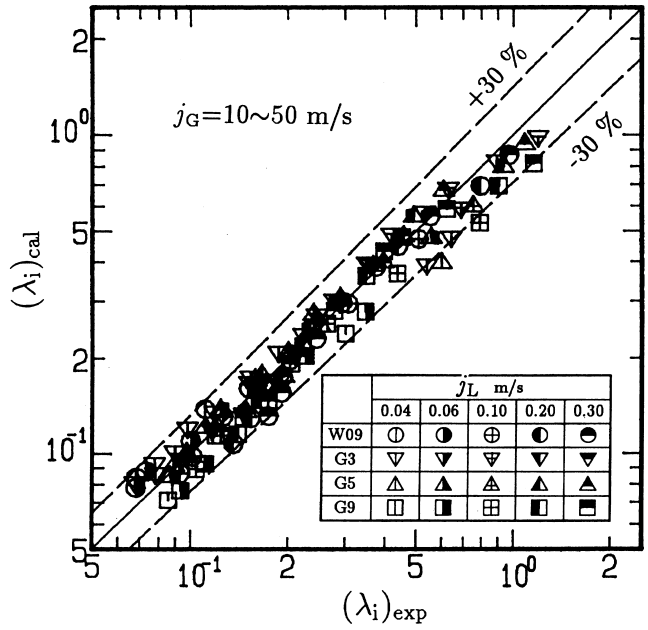

Figure 13. Comparison between the measured and the calculated interfacial friction factor.

$$\lambda_i = \lambda_S\{1 + 6.1 \times 10^{-5} X^{0.52}(\Gamma/\nu_L)^{0.65} Re_{GO}^{0.7}\} \quad [18]$$

Where λ_S is the friction factor for a gas single phase flow, X the Martinelli parameter, and Γ the volume flow rate of liquid per unit width. The difference between λ_i given by [18] and the experimental data is significantly large in small Re_{GO} region, and gradually becomes small as Re_{GO} increases, and finally both values approximately agree in the region of $Re_{GO} \geq 5 \times 10^4$. Such a trend is considered to be caused by the fact that the interfacial wavy characters, closely related to λ_i, are strongly dependent upon the mean liquid film thickness. It is controlled mainly by the interfacial shear stress in the case of horizontal flow, and by gravity in the case of vertical flow. In short, the large difference is caused by the gravitational force in small Re_{GO} region.

To estimate λ_i for a vertical annular flow, the we proposed a following correlation which was obtained by trial and error.

$$\lambda_i = 1.7(12 + \nu_L/\nu_W)^{-1.33}\{1 + 12(t_{fm}/D)\}^8 \quad [19]$$

This correlation has a considerably large power of 8. We tried to use the term $\{1 + 96\ (t_{fm}/D)\}$ in [19] instead of the term $\{1 + 12\ (t_{fm}/D)\}^8$, because $12\ (t_{fm}/D)$ is less than 0.75 in the present experimental range. However, it could not express the sharp increase of the λ_i in the larger (t_{fm}/D) range. Therefore we proposed the above [19]. Where ν_W is the kinematic viscosity of water at 20°C. Figure 13 shows the comparison of λ_i estimated by [19] with the measured values of λ_i for all the experimental points. The data is correlated within an accuracy of ±30% regardless of ν_L, j_G, and j_L. Where the correlation (9) is used to determine t_{fm}/D in [19].

3.5. *Prediction method of frictional pressure drop*

Substituting $\bar{u}_G = j_G/\hat{\alpha}$, $\hat{\alpha} = (D_i/D)^2$ and $D_i = D - 2t_{fm}$ into [13], the pressure drop $-dp/dz$ is expressed by the following equation:

$$-\frac{dp}{dz} = \frac{\lambda_i}{2D}\frac{j_G^2}{\{1 - 2(t_{fm}/D)\}^5}\rho_G \quad [20]$$

This equation means that the frictional pressure drop $(-dp/dz)$ is determined if t_{fm}/D and λ_i are given. We propose to use [9] and [19] for them. If j_G, j_L tube diameter D, and physical prop-

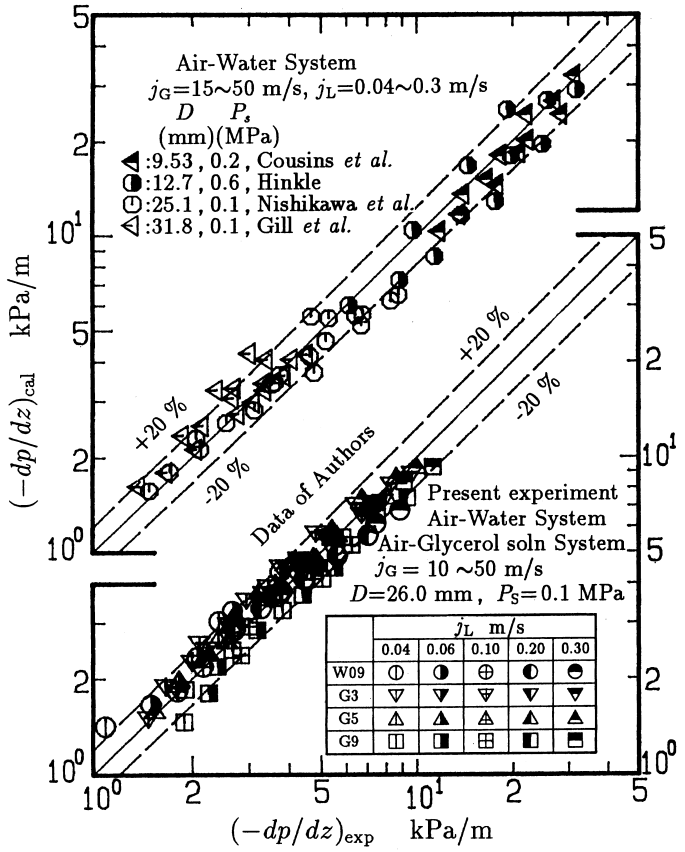

Figure 14. Comparison between the predicted and the measured pressure drops.

erties of fluid (v_L, ρ_L, ρ_G) are given, as well as the flow conditions j_G and j_L, the frictional pressure drop can be estimated by [20].

Comparison of predicted values for the pressure drops obtained from this prediction method, $(-dp/dz)_{cal}$, and the measured values $(-dp/dz)_{exp}$ is shown in figure 14. The result in the lower part of this figure shows the present experimental data. As seen in figure 14, the predicted values agree with the measured data within an accuracy of $\pm 20\%$ independently of v_L.

Similar comparisons were also done for experimental data measured by other researchers, i.e., Cousins *et al.* (1965), Hinkle (1967), Nishikawa *et al.* (1967), and Gill *et al.* (1964) and are shown in the upper part of figure 14. Experimental data has been obtained in the vertical upward annular flow of air and water at room temperature under the conditions of wide ranges of the tube diameter (9.53 ~ 31.8 mm) and the system pressure ($P_S = 0.1 \sim 0.6$ MPa). Figure 14 shows that the measured values in those cases are also estimated by [20] within an accuracy of $\pm 20\%$ regardless of tube diameter and system pressure as is the case of our experiment, where the change of liquid viscosity is taken into account. Figure 14 also verifies that τ_i obtained in the our experiment is reasonable although considerably larger than that found in the correlations by Wallis (1969) and Moeck (1970).

From the investigation described above, we can conclude that the prediction method proposed in this paper is applicable in the range of values described above with a satisfactory accuracy.

4. CONCLUSIONS

The experiments were carried out on the isothermal annular two-phase upwards flow in a vertical tube with the inner diameters of 26.0 mm and 19.2 mm for air–water and air–aqueous glycerol solution systems, to clarify the effects of liquid viscosity on the interfacial structures, the mean liquid film thicknesses t_{fm}, the wave height h, and the interfacial friction factors λ_i. The

prediction method of the frictional pressure drops ($-dp/dz$) is also proposed. The main results obtained are summarized as follows:

1. By observation of the shape of waves of the liquid holdup signals, and the still photographs of gas–liquid interfaces it is clarified that the interfacial structure is strongly depend on the liquid viscosity.
2. As liquid viscosity increases, the interfacial friction factor decreases if compared under the same mean liquid film thickness, but increases under the same Reynolds number of gas phase.
3. We proposed [9] and [19], respectively, for correlations of the mean liquid film thickness and the interfacial friction factor in the annular flow, in which the change in the liquid viscosity is taken into consideration.
4. We proposed a method to predict the frictional pressure drop by using [9] and [19] in [20]. In this method the only information needed is the superficial gas and liquid velocities if the inner diameter of tube, and fluids properties (liquid viscosity, densities of gas and liquid) are known.

Acknowledgements—The authors express their appreciation to I. Moriwaki and K. Nanri (students of Sasebo College of Technology at that time) for their cooperation in the experiment.

REFERENCES

Abolfadl, M. and Wallis, G. B. (1986) An improved mixing-length model for annular two-phase flow with liquid entrainment. *Nuclear Engineering and Design* **95,** 233–241.

Ambrosini, W., Andreussi, P. and Azzopardi, J. (1991) A physically based correlation for drop size in annular flow. *Int. J. Multiphase Flow* **17** (4), 497–507.

Asali, J. C., Hanratty, T. J. and Andreussi, P. (1985) Interfacial drag and film height for vertical annular flow. *AIChE J.* **31,** 895–902.

Baker, O. (1954) Simultaneous flow of oil and gas. *Oil and Gas J.* **53,** 185–190.

Cousins, L. B., Dencon, W. H. and Hewitt, G. F. (1965) Liquid mass transfer in annular two-phase flow. *Paper C4, Symposium on Two-phase Flow*, University of Exeter, Vol. 2, pp. C401–C430, England, June 1965.

Fukano, T. (1997) Measurement of time varying thickness of liquid film flowing with high speed gas flow by a constant electric current method (CECM). *Proc. of OECD/CSNI Specialist Meeting on Advanced Instrumentation and Measurement Techniques, Santa Barbara.*

Fukano, T., Itoh, A., Odawara, H., Kuriwaki, T. and Takamatu, Y. (1985) liquid films flowing concurrently with air in horizontal duct (5th report, interfacial shear stress). *Bull. of JSME* **28** (244), 2294–2301.

Fukano, T., Ousaka, S., Morimoto, T. and Sekoguchi, K. (1983) Air-water annular two-phase flow in a horizontal tube (2nd report: circumferential variation of film thickness parameters). *Bull. of JSME* **26** (218), 1387–1395.

Furukawa, T. (1995) Effect of liquid viscosity on liquid-lump velocity in vertical-upward gas-liquid two-phase flow (velocity characteristics of the long-life liquid lump). *Jap. J. Multiphase Flow* **9** (2), 121–131.

Furukawa, T. and Fukano, T. (1996) Effect of liquid viscosity on flow pattern in vertical upward gas-liquid two-phase flow. *Trans. Jap. Soc. Mech. Eng.*, **62**-601, B, 3257–3264.

Gill, L. E., Hewitt, G. F. and Lacey, P. M. G. (1964) Sampling probe studies of the gas core in annular two-phase flow. Part II. studies of the effect of phase flow rates on phase and velocity distribution. *Chem. Eng. Science* **19,** 665–682.

Gill, L. E., Hewitt, G. F. and Roberts, D. N. (1969) Studies of the behaviour of disturbance waves in annular flow in a long vertical tube. UKAEA report AERE-R6012.

Hinkle, W. D. (1967) A study of liquid mass transport in annular air–water flow. *Sc.D. Thesis, Department of Nuclear Engineering*, M.I.T.

Hori, K., Nakasatomi, M., Nishikawa, K. and Sekoguchi, K. (1978) Study of ripple region in annular two-phase flow (3rd report, effect of liquid viscosity on gas–liquid interfacial character and friction factor). *Trans. Jap. Soc. Mech. Eng*., **44**-387, 3847–3856.

Jensen, M. K. (1987) The liquid film and the core region velocity profiles in annular two-phase flow. *Int. J. Multiphase Flow* **13** (5), 615–628.

Kosky, P. G. (1971) Thin liquid films under simultaneous shear and gravity forces. *Int. J. Heat Mass Transfer* **14,** 1120–1224.

Leman, G. W. (1983) Effect of liquid viscosity in two-phase annular flow. M.S. Thesis, Univ. of Illinois, Urbana.

Leman, G. W. (1985) Atomization and deposition in two-phase annular flow: measurement and modeling. Ph.D. thesis, Dept of Chem. Engng, Univ. of Illinois, Urbana.

Moeck, E. O. (1970) Annular-dispersed two-phase flow and critical heat flux. *AECL*, 3656.

Nishikawa, K., Sekoguchi, K., Nakasamomi, M. and Kaneuzi, A. (1967) Liquid film flow in upwards two-phase flow. *JSME Semi-International Symposium*, 4th–8th September Tokyo, pp. 65–74.

Skouloudis, A. N. and Würtz, J. (1993) Film-thickness, pressure-gradient, and turbulent velocity profiles in annular dispersed flow. *J. Fluids Eng*. **115,** 265–269.

Wallis, G. B. (1969) Annular two-phase flow-part II (additional effects). *ASME Paper*, 69 = FE-46.

Whalley, P. B., Hewitt, G. F. and Hutchinson, P. (1973) Experimental wave and entrainment measurements in vertical annular two-phase flow. AERE Report R7521.

Whalley, P. B. and Hewitt, G. F. (1978) The correlations of liquid entrainment fraction and entrainment rate in annular two-phase flow. UKAEA Report AERE-R9187.

Willetts, I. P. (1987) Non-aqueous annlar two-phase flow. Ph.D. Thesis, Univ. of Oxford, U.K.